Structural ordering and symmetry breaking in $Cd_2Re_2O_7$

J. P. Castellan,[1] B. D. Gaulin,[1,4] J. van Duijn,[1] M. J. Lewis,[1] M. D. Lumsden,[2] R. Jin,[2] J. He,[3] S. E. Nagler,[2] and D. Mandrus[2,3]

[1]*Department of Physics and Astronomy, McMaster University, Hamilton, Ontario, Canada L8S 4M1*

[2]*Solid State Division, Oak Ridge National Laboratory, P. O. Box 2008, Oak Ridge, Tennessee 37831*

[3]*Department of Physics and Astronomy, The University of Tennessee, Knoxville, Tennessee 37996*

[4]*Canadian Institute for Advanced Research, 180 Dundas Street W., Toronto, Ontario, Canada M5G 1Z8*

(Received 23 August 2002; published 30 October 2002)

Single-crystal x-ray-diffraction measurements have been carried out on $Cd_2Re_2O_7$near and below the phase transition it exhibits at $T_{C'} \sim 195$ K. $Cd_2Re_2O_7$ was recently discovered as the first, and to date only, superconductor that displays the cubic pyrochlore structure at room temperature. Superlattice Bragg peaks show an apparently continuous structural transition at $T_{C'}$, however, their behavior is unconventional. The evolution with temperature of these Bragg intensities show anomalously strong temperature dependence at low temperatures, where it falls off as $I_0(1-BT^2)$, and resolution limited critical-like scattering is seen above $T_{C'}$. High-resolution measurements show that the high-temperature cubic Bragg peaks split on entering the low-temperature phase, indicating a (likely tetragonal) lowering of symmetry below $T_{C'}$.

DOI: 10.1103/PhysRevB.66.134528 PACS number(s): 74.70.−b, 61.10.−i, 64.70.Kb

I. INTRODUCTION

Materials which crystallize into the cubic pyrochlore structure have been of intense recent interest, due to the presence of networks of corner-sharing tetrahedra within such structures.[1] Cubic pyrochlores display chemical composition $A_2B_2O_7$ and space group $Fd\bar{3}m$. Independently, both the *A* and *B* sublattices reside on networks of corner-sharing tetrahedra, an architecture also common to the Laves phase cubic spinels, for example. Such materials have the potential to display phenomena related to geometrical frustration in the presence of antiferromagnetism. While much activity has focused on local magnetic moments in insulating pyrochlores, interesting metallic properties have also been observed recently. The $RE_2Mo_2O_7$ system (where RE is a rare-earth ion), for example, is well studied and is known to undergo a transition from metallic ferromagnetism to semiconducting spin-glass behavior as one moves from the light to the heavy rare earths occupying the *A* sublattice of the pyrochlore structure.[2] One such metallic pyrochlore $Nd_2Mo_2O_7$ (Ref. 3) has recently been seriously studied and a large anomalous Hall effect has been measured. In $Cd_2Os_2O_7$, a metal-insulator transition has recently been shown to occur near 226 K,[4] while the spinel LiV_2O_4 is the only known transition-metal-based heavy fermion conductor.[5]

While many metallic, cubic pyrochlore oxides exist, no superconductors were known to exist within this family of materials until very recently. Hanawa *et al.*,[6] Sakai *et al.*,[7] and Jin *et al.*[8] have all recently reported on the superconductivity in $Cd_2Re_2O_7$, the first such pyrochlore. The superconducting T_C's are somewhat sample dependent and have been reported between 1 and 2 K. Moreover, the high-temperature metallic properties are anomalous, and may be driven by an as yet poorly understood phase transition near $T_{C'} \sim 195$ K.[9] In this paper, we report on the nature of the phases above and below $T_{C'}$ as well as the phase transition itself. We show compelling evidence for a splitting of the cubic Bragg peaks, indicating a lowering of symmetry below $T_{C'}$, likely to a tetragonal structure, as well as an unusual order parameter that grows very slowly with decreasing temperature.

$Cd_2Re_2O_7$is a rather poor metal near room temperature, exhibiting an almost flat resistivity between 200 K and 400 K.[6,7,9] Just below 200 K, the resistivity falls off sharply, continuing down to a low-temperature Fermi-liquid regime characterized by a T^2 dependence to the resistivity between 2 K and roughly 60 K, and a residual resistivity of the order of 10 $\mu\Omega$ cm.[6,8] On further lowering the temperature, the resistivity falls to zero, at $T_C \sim 1.4$ K in crystals from the same batch as that under study here, indicating the onset of the superconducting state. Heat-capacity measurements show a large anomaly at T_C, while above T_C these measurements give a Sommerfeld γ value of roughly 30 mJ/mol K^2. This result can be combined with *A*, the coefficient of the quadratic term in the temperature dependence of the resistivity, to give a Kadowaki-Woods ratio A/γ, similar to that seen in highly correlated metals such as the heavy-fermion superconductor UBe_{13}.[8] Recent transverse field μSR measurements[10] reveal the presence of a vortex lattice below T_C, with a large and temperature independent value of the penetration depth below $0.4T_C$. These measurements show $Cd_2Re_2O_7$to be a type-II superconductor, and are consistent with a nodeless superconducting energy gap.

Heat-capacity measurements show a pronounced anomaly near $T_{C'} \sim 200$ K, consistent with a continuous phase transition.[9] Electron diffraction from single crystals[9] and preliminary x-ray-diffraction studies from powder samples[11] show the appearance of superlattice Bragg peaks at reflections such as (0,0,6) and (0,0,10), which are inconsistent with the $(0,0,h)$: $h=4n$ condition appropriate to the high-temperature cubic space group. In addition, dc susceptibility measurements[6,9] show an abrupt reduction in the susceptibility below $T_{C'}$. Very recent Re nuclear quadrupole resonance (NQR) measurements, however, have revealed no indication of either a magnetically ordered or a charge ordered state below 100 K.[12]

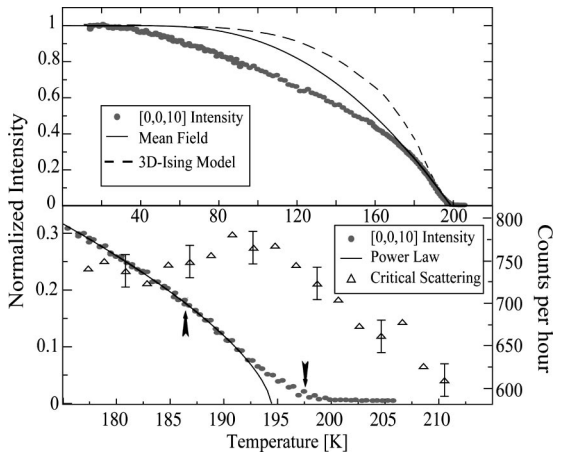

FIG. 1. The top panel shows the integrated intensity of the (0,0,10) superlattice Bragg peak as a function of temperature, compared with the square of the order parameter expected from mean-field theory, and that expected from the three-dimensional Ising model. The lower panel shows the same data in the immediate vicinity of $T_{C'} \sim 194$ K, along with a fit to critical behavior modeled as a power law in reduced temperature (left-hand *y* axis), and the broad critical scattering as measured at (0.04,0.064,10) (right-hand *y* axis).

II. EXPERIMENTAL DETAILS

The high-quality single crystal, which is the subject of the present study, was grown as reported by He *et al.*,[13] and had approximate dimensions of $4\times4\times2$ mm^3 and a mosaic spread of less than 0.04° full width at half maximum. It was mounted in a Be can in the presence of a He exchange gas and connected to the cold finger of a closed cycle refrigerator with approximate temperature stability of 0.005 K near $T_{C'}$, and 0.01 K elsewhere. X-ray-diffraction measurements were performed in two modes, both employing an 18-KW rotating anode generator, Cu $K\alpha$ radiation, and a triple-axis diffractometer. Relatively low-resolution measurements of the superlattice Bragg-peak intensities were obtained using a pyrolitic graphite (002) monochromator and a scintillation counter. Much higher resolution measurements were performed with a perfect Ge (111) monochromator, and a Bruker Hi Star area detector, mounted 0.75 m from the sample position on the scattered beam arm of the diffractometer. The high-resolution experiment easily separated Cu $K\alpha_1$ from Cu $K\alpha_2$ diffraction, and was used for precision measurements of the line shapes of both the principal and superlattice Bragg peaks.

III. ORDER PARAMETER

Figure 1 shows the temperature dependence of the integrated intensity of low-resolution scans of the (0,0,10) superlattice Bragg peak. Data were taken in separate warming and cooling runs, and are shown over an extended temperature range in the top panel, as well as over a narrow range near $T_{C'}$ in the bottom panel. The form of this scattering, proportional to the square of the order parameter, is anomalous as it grows very slowly below $T_{C'}$, especially between $\sim$170 K and $\sim$40 K. A mean-field phase transition displays the slowest such growth among conventional models for cooperative behavior, which exhibit continuous phase transitions. In Fig. 1, we compare the integrated intensity of the superlattice Bragg scattering to the square of the mean-field order parameter,[14] as well as to the square of the order parameter appropriate to the three-dimensional Ising model.[15] Clearly the growth of the measured order parameter is much slower with decreasing temperature, than would be predicted by even mean-field theory.

Closer to the phase transition, the measured order parameter does look more conventional as shown in the bottom panel of Fig. 1. This panel shows integrated intensity with both downward curvature below $\sim$195 K and upward curvature above $\sim$195 K, consistent with the measurement of the order parameter squared below $T_{C'}$, and the measurement of fluctuations in the order parameter (or so-called critical scattering) above $T_{C'}$. Data in the temperature range 175–190 K were analyzed assuming this to be the case, and fits were carried out in the approximate range of reduced temperature from 0.02 to 0.10, placing the data within a typical asymptotic critical regime. The fit of this data by the critical form

$$\text{Intensity} = I_0\left(\frac{T_{C'}-T}{T_{C'}}\right)^{2\beta} \tag{1}$$

is shown in the bottom panel of Fig. 1. The fit is of high quality, and it produces $T_{C'} = 194.3 \pm 0.1$ K and a critical exponent $\beta = 0.33 \pm 0.03$, which is typical of three-dimensional continuous phase transitions.[16]

Although the (0,0,10) intensity above $T_{C'} = 194.3$ appears to be critical scattering, we show below that it is anomalous and remains resolution limited at all temperatures measured. **Q**-broadened critical fluctuations can be measured by moving slightly off the (0,0,10) Bragg position, however, it is extremely weak. Scattering at (0.04,0.064,10) is shown in the bottom panel of Fig. 1, and it displays a weak peak near $T_{C'}$, as expected for a continuous phase transition. This broad scattering is measured in counts per hour, and it makes a negligible contribution to the overall scattering around (0,0,10) above $T_{C'} = 194.3$. It does, however, provide a consistency check on the phase transition occurring at 194.3 K.

High-resolution measurements of the line shape of the (0,0,10) superlattice Bragg peak, shown in Fig. 2, reveal that almost all of the this scattering above $T_{C'} = 194.3$ K remains resolution limited; it is indistinguishable from the superlattice scattering below 194.3 K, albeit weaker in intensity. Figure 2 shows maps of the scattering at and around the (0,0,10) superlattice position at temperatures of 185.7 K and 197.4 K. As indicated by the arrows superposed on the order parameter shown in the bottom panel of Fig. 1, these temperatures correspond to well below and well above $T_{C'}$.

The 197.4-K data set definitely falls within the upward curvature regime of the temperature dependence of the superlattice integrated intensity, and would normally be expected to be due to fluctuations in the order parameter rather than due to the order parameter itself. As discussed above, such critical scattering is expected to broaden in **Q**, and

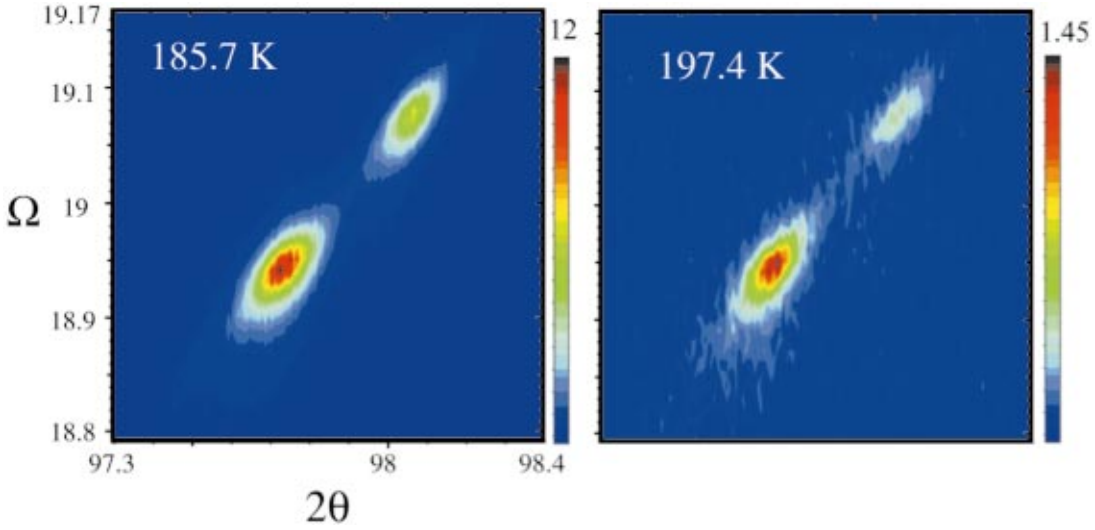

FIG. 2. (Color) High-resolution scans of the scattering at and near the (0,0,10) superlattice Bragg-peak positions are shown for the temperatures marked by arrows in the inset to Fig. 1. Data are shown in maps as a function of sample rotation angle Ω and scattering angle 2θ. The two diffraction features at 2θ values of $\sim$97.7° and 98.07° are from Cu $K\alpha 1$ and Cu $K\alpha 2$ radiations, respectively. The top of the linear color scale is different for each dataset.

therefore in angular coordinates, as the temperature increases beyond $T_{C'}$, indicating a finite and decreasing correlation length. Such broadening is clearly not observed in this scattering above $T_{C'}$.

The anomalous nature of the line shape of the superlattice scattering above $T_{C'}$ may be due to "second length scale" scattering,[17] which has often been observed in high-resolution synchrotron x-ray experiments near phase transitions in crystalline materials. It is not fully understood, but has been associated with the effect of near-surface quenched disorder on the phase transition. The x rays in the present measurements have a penetration depth of the order of 10 μm (tens of thousands of unit cells) and are thus not particularly surface sensitive.

It may also be that this superlattice Bragg scattering is not the primary order parameter for the phase transition near $T_{C'}$, but is a secondary feature, pulled along by the true underlying phase transition. The anomalously slow growth of the (0,0,10) superlattice Bragg peak at low temperatures also supports such an interpretation.

IV. LATTICE PARAMETERS

We also carried out measurements of the principal Bragg peaks [which satisfy the (00h): $h=4n$ relation] at high scattering angle and in high-resolution mode. Scans along the longitudinal direction, cutting through both Cu $K\alpha_1$ and Cu $K\alpha_2$ peaks of the (0,0,12) principal Bragg peaks, are shown in the right-hand panels of Fig. 3 on a linear scale, and in the bottom, left panel of Fig. 3 on a semilog scale. For comparison, similar longitudinal scans through the superlattice (0,0,10) Bragg peaks are shown on a semilog scale in the top left panel of Fig. 3. The datasets at the two temperatures that make up both semilog plots on the left side of Fig. 3 have been shifted slightly in 2θ and, in the case of (0,0,10), scaled in intensity to allow for comparison.

A shoulder is clearly seen to develop on the high angle side of the (0,0,12) peaks as the temperature is lowered below $T_{C'}$. This indicates a splitting of the cubic Bragg peak into a line shape characterized by at least two different lattice parameters, and consequently a symmetry lower than cubic (likely tetragonal) in the low-temperature state below $T_{C'}$ $\sim$194.3 K.

A similar splitting of the (0,0,10) superlattice Bragg peak is *not* observed. The superlattice Bragg peaks do not exist above $T_{C'}$ and thus we must compare superlattice data taken below, but near $T_{C'}$ with that taken well below $T_{C'}$. That is

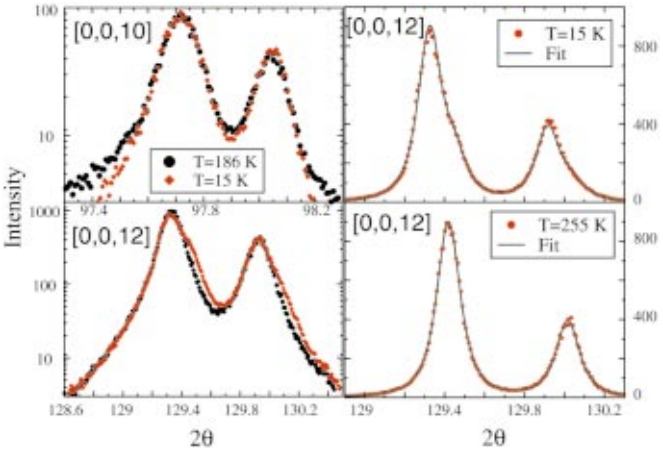

FIG. 3. (Color) The right hand panels shows longitudinal cuts taken through the (0,0,12) principal Bragg peak position well above $T_{C'}$ (bottom) and well below (top). This data, on a linear scale, shows a clear shoulder on the high 2θ side of both the Cu $K_{\alpha 1}$ and $K_{\alpha 2}$ peaks. The left hand panels show the superlattice (0,0,10) (top) and principal (0,0,12) (bottom) Bragg peaks on a semi-log scale, at temperatures just below and well below $T_{C'}$. Clearly, while the principal Bragg peaks split on lowering the temperature, the superlattice peaks do not.

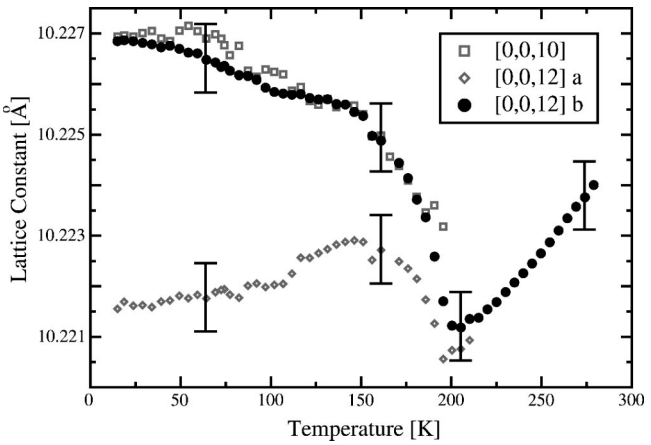

FIG. 4. The temperature dependence of the lattice parameters extracted from fits to the (0,0,12) principal Bragg peaks is shown along with the temperature dependence of the superlattice (0,0,10) Bragg-peak periodicity below $T_{C'}$. The error bars indicate uncertainties associated with the absolute values of the lattice parameters.

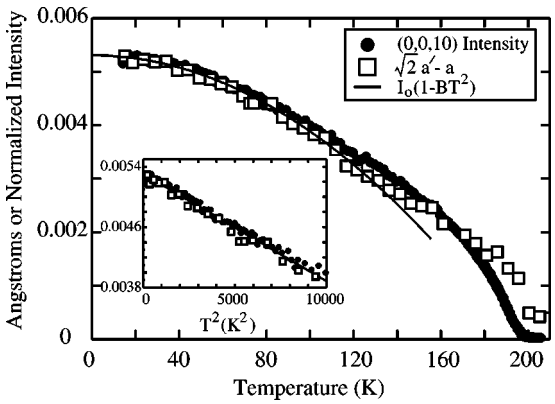

FIG. 5. The temperature dependence of the lattice parameters extracted from fits to the (0,0,12) principal Bragg peaks is shown, along with the temperature dependence of the superlattice (0,0,10) Bragg peak intensity below $T_{C'}$.

what is shown for both the principal (0,0,12) Bragg peak and the superlattice (0,0,10) Bragg peak at temperatures of 186 K and 15 K, respectively, in the left-hand panels of Fig. 3. At 186 K, the splitting is not yet evident in either the principal, (0,0,12), or superlattice, (0,0,10), Bragg peaks, but by 15 K it is clear in the principal Bragg peak, but not in the superlattice Bragg peaks.

We fit the high-temperature data at (0,0,12) to a phenomenological form at 255 K, assuming this to be the resolution-limited line shape. We then fit (0,0,12) data at all temperatures to a form assuming the superposition of two such line shapes, displaced from each other in scattering angle (2θ). This protocol allowed us to extract peak positions for each of the two peaks, giving the lattice parameters as a function of temperature. This analysis assumes that only two lattice parameters are present at low temperatures, that is, the low-temperature structure is tetragonal. The data at 15 K in the top right panel of Fig. 3 shows the quality of this fit, and clearly the description of the data is very good. The resulting tetragonal lattice parameters as a function of temperature are shown in Fig. 4.

V. DISCUSSION

The behavior of the lattice parameters as a function of temperature is striking. The cubic lattice parameter displays the usual thermal contraction with decreasing temperature until near $T_{C'}$. The splitting in the lattice parameters first develops near 200 K, with a 30-K interval from ~190 K to 160 K in which both lattice parameters increase with decreasing temperature. This trend continues to lower temperatures for the larger of the two lattice parameters, while the smaller turns over below ~150 K and displays relatively weak contraction to lower temperatures. At the lowest temperature measured, 15 K, the maximum splitting in lattice parameter measured is about 0.005 Å or 0.05%. The (0,0,10) superlattice peak does not show any splitting, and the temperature dependence associated with its periodicity is also shown in Fig. 4. It clearly follows the upper branch of the two lattice parameters associated with (0,0,12). These results imply that the low-temperature state below $T_{C'}$ is likely twinned tetragonal, such that two of (0,0,12), (0,12,0), and (12,0,0) have one lattice parameter, while the other has a slightly different one. The fact that the superlattice peak displays no splitting implies that only the subset of (0,0,10), (0,10,0), and (10,0,0), which follow the upper branch of the lattice parameter vs temperature curve shown in Fig. 4, exists. The other(s) is (are) systematically absent. These observations allow us to discuss possible tetragonal space groups appropriate to the low-temperature state below $T_{C'}$. As the transition appears to be close to continuous, we assume the low-temperature state to be a gradual distortion of the high-temperature cubic state, and thus the low-temperature space group should be a subgroup of $Fd\bar{3}m$. There are two body-centered subgroups of $Fd\bar{3}m$ which, in the presence of twinning, would split (0,0,12) and allow a single periodicity for (0,0,10). These are $I4_1$ and $I4_122$. In both cases the primitive unit vectors of the basal $(a'\text{-}a')$ plane are rotated by 45° relative to the unit vectors a of the high temperature cubic unit cell, and $a' = a/\sqrt{2}$.

We return now to the question of the anomalously strong temperature dependence of the superlattice Bragg-peak intensity at low temperatures. In Fig. 5 we compare the temperature dependence of the (0,0,10) superlattice intensity with the difference between the lattice parameters $\sqrt{2}a' - a$, taken from the analysis leading to Fig. 4. Figure 5 shows clearly that the same anomalous temperature dependence is seen in both the superlattice Bragg-peak intensity and in $\sqrt{2}a' - a$. This is certainly surprising as the superlattice Bragg-peak intensity is associated with the *square* of the order parameter in most structural phase transitions, while the difference in lattice parameter, $\sqrt{2}a' - a$, is most naturally taken as the order parameter itself.

This result suggests that the temperature dependence of both the superlattice Bragg intensity and the difference in lattice parameter are driven by the same physical origin, at least at low temperatures. Over the temperature range from low temperatures until almost 100 K, both quantities are well

described by $I_0(1-BT^2)$. This quadratic temperature dependence was fitted to the data and is shown in Fig. 5 as a solid line. The inset of Fig. 5 shows both the (0,0,10) intensity and $\sqrt{2}a'-a$ plotted as a function of the temperature being squared. There is no doubt that the decay of both the difference in lattice parameter and the superlattice intensity goes as T^2 at low temperatures. As the low-temperature resistivity of this material displays the Fermi-liquid behavior and goes like T^2 to temperatures as high as 60 K, an electronic origin for the low-temperature behavior of the evolving structure is very strongly suggested. Given that the electronic properties are strongly correlated to the structural phase transition at $T_{C'}$, it is perhaps not so surprising that such a strong correlation is evident at low temperatures as well.

VI. SUMMARY

While we cannot be more precise as to the low-temperature space group at this time, we have unambiguously shown the symmetry of the low-temperature state to be lower than cubic, and that this cubic symmetry breaking is an essential feature of the phase transition. The most likely scenario is that $Cd_2Re_2O_7$undergoes a cubic to tetragonal phase transition, with the primary order parameter being the difference in lattice parameters, given by $\sqrt{2}a'-a$. We note that we do not expect this splitting of the lattice parameters to be evident in bulk measurements unless a single-domain sample can be produced at low temperatures.

We have also shown that the superlattice Bragg-peak intensities display anomalously strong temperature dependence at low temperature, going like $I_0(1\text{-}BT^2)$ at temperatures below $\sim$100 K. These results indicate a strong coupling between the electronic properties and the evolving structure at all temperatures below $T_{C'}=194.3$ K.

Finally, it is interesting to note that recent theoretical work may have anticipated such a structural phase transition related to the underlying network of corner-sharing tetrahedra. This work[18] discusses the role of magnetoelastic couplings in generating ''order by distortion'' in pyrochlore antiferromagnets.

ACKNOWLEDGMENTS

We wish to acknowledge useful discussions with J. F. Britten. This work was supported by the NSERC of Canada. Oak Ridge National Laboratory is managed by UT-Battelle, LLC, and the U.S. Department of Energy under Contract No. DE-AC05-00OR22725. Work at UT was supported by the NSF Grant No. DMR-0072998.

[1] For recent reviews, see S.T. Bramwell and M.J.P. Gingras, Science **294**, 1495 (2001); *Magnetic Systems with Competing Interactions*, edited by H.T. Diep (World Scientific, Singapore, 1994); P. Schiffer and A.P. Ramirez, Comments Condens. Matter Phys. **18**, 21 (1996).

[2] N. Ali, M.P. Hill, S. Labroo, and J.E. Greedan, J. Solid State Chem. **83**, 178 (1989); T. Katsufuji, H.Y. Hwang, and S.-W. Cheong, Phys. Rev. Lett. **84**, 1998 (2000).

[3] Y. Taguchi, Y. Oohara, H. Yoshizawa, N. Nagaosa, and Y. Tokura, Science **291**, 2573 (2001).

[4] D. Mandrus, J.R. Thompson, R. Gaal, L. Forro, J.C. Bryan, B.C. Chakoumakos, L.M. Woods, B.C. Sales, R.S. Fishman, and V. Keppens, Phys. Rev. B **63**, 195104 (2001).

[5] S. Kondo, D.C. Johnston, C.A. Swenson, F. Borsa, A.V. Mahajan, L.L. Miller, T. Gu, A.I. Goldman, M.B. Maple, D.A. Gajewski, E.J. Freeman, N.R. Dilley, R.P. Dickey, J. Merrin, K. Kojima, G.M. Luke, Y.J. Uemura, O. Chmaissem, and J.D. Jorgensen, Phys. Rev. Lett. **78**, 3729 (1997); C. Urano, M. Nohara, S. Kondo, F. Sakai, H. Takagi, T. Shiraki, and T. Okubo, *ibid.* **85**, 1052 (2000).

[6] M. Hanawa, Y. Muraoka, T. Tayama, T. Sakakibara, J. Yamaura, and Z. Hiroi, Phys. Rev. Lett. **87**, 187001 (2001).

[7] H. Sakai, K. Yoshimura, H. Ohno, H. Kato, S. Kambe, R.E. Walstedt, T.D. Matsuda, Y. Haga, and Y. Onuki, J. Phys.: Condens. Matter **13**, L785 (2001).

[8] R. Jin, J. He, S. McCall, C.S. Alexander, F. Drymiotis, and D. Mandrus, Phys. Rev. B **64**, 180503(R) (2001).

[9] R. Jin, J. He, J.R. Thompson, M.F. Chrisholm, B.C. Sales, and D. Mandrus, cond-mat/0108402 (unpublished).

[10] M.D. Lumsden, S.R. Dunsiger, J.E. Sonier, R.I. Miller, R.F. Kiefl, R. Jin, J. He, D. Mandrus, S.T. Bramwell, and J.S. Gardner, cond-mat/0111187 (unpublished); R. Kadono, W. Higemoto, A. Koda, Y. Kawasaki, M. Hanawa, and Z. Hiroi, cond-mat/0112448 (unpublished).

[11] M. Hanawa, J. Yamaura, Y. Muraoka, F. Sakai, and Z. Hiroi, cond-mat/0109050 (unpublished).

[12] O. Vyaselev, K. Arai, K. Kobayashi, J. Yamazaki, K. Kodama, M. Takigawa, M. Hanawa, and Z. Hiroi, Phys. Rev. Lett. **89**, 017001 (2002).

[13] J. He *et al.* (unpublished).

[14] M. Plischke and B. Birgerson, *Equilibrium Statistical Physics*, 2nd ed. (World Scientific, Singapore, 1994).

[15] D.M. Burley, Philos. Mag. **5**, 909 (1960).

[16] M.F. Collins, *Magnetic Critical Scattering* (Oxford University Press, London, 1989).

[17] For example, S.R. Andrews, J. Phys. C **19**, 3721 (1986); T.R. Thurston, G. Helgesen, Doon Gibbs, J.P. Hill, B.D. Gaulin, and G. Shirane, Phys. Rev. Lett. **70**, 3151 (1993).

[18] O. Tchernyshyov, R. Moessner, and S.L. Sondhi, Phys. Rev. Lett. **88**, 067203 (2002).